International Journal of Speleology	53 (2)	235-251	Tampa, FL (USA)	June 2024

Available online at scholarcommons.usf.edu/ijs

International Journal of Speleology

Official Journal of Union Internationale de Spéléologie

Manifestations of sulfuric acid speleogenesis in the Mulapampa travertine, Central Andes of Peru: evidence from the Gruta con Lago

Andrzej Tyc [1], Krzysztof Gaidzik [1], Justyna Ciesielczuk [1], and Katarzyna Wątor [2]

[1]Institute of Earth Sciences, Faculty of Natural Sciences, University of Silesia in Katowice, Będzińska 60, 41-200 Sosnowiec, Poland
[2]AGH University of Kraków, Mickiewicza 30, 30-059 Kraków, Poland

Abstract: Sulfuric acid speleogenesis (SAS) is a form of hypogene speleogenesis characterized by the formation of caves in carbonate rocks due to the presence of sulfuric acid. This study focuses on the Gruta con Lago, one of three caves identified in the Mulapampa travertine, located in the Central Andes of Peru. These caves are accessed through collapse sinkholes, and much of their morphology results from roof breakdown. The bottom of the studied cave is situated at the current water table. Despite the absence of typical solutional features associated with SAS caves, mineralogical and geochemical evidence of speleogenesis involving H_2SO_4 has been found in Gruta con Lago. Significant accumulations of gypsum deposits on the cave floor and replacement gypsum crusts on walls – both considered by-products of SAS – are present. Cave gypsum samples exhibit negative sulfur isotopic composition (ranging from -19.4 to -8.2‰) and oxygen (ranging from -9.0 to -1.3‰), which are indicative of sulfide (H_2S) oxidation. This article discusses potential scenarios of SAS events in the evolution of hypogene karst in the Mulapampa travertine. It also considers the significance of the proximity of the active volcanoes of the Ampato-Sabancaya Volcanic Complex (ASVC) and seismogenic crustal faults in the formation of a thick travertine cover and the potential for SAS processes.

Keywords: hypogene karst, sulfur stable isotopes, travertine, Central Andes, Peru

Received 28 February 2024; Revised 23 September 2024; Accepted 16 October 2024

Citation: Tyc, A., Gaidzik, K., Ciesielczuk, J., Wątor, K., 2024. Manifestations of sulfuric acid speleogenesis in the Mulapampa travertine, Central Andes of Peru: evidence from the Gruta con Lago. International Journal of Speleology, 53(2), 235-251. https://doi.org/10.5038/1827-806X.53.2.2503

INTRODUCTION

Sulfuric acid speleogenesis (SAS) is a distinct form of hypogene speleogenesis, in which the caves are primarily formed by the interaction of sulfuric acid with the carbonates. This acid is produced by the abiotic or/and biotic oxidation of solid or aqueous-phase sulfides, with hydrogen sulfide (H_2S) being the most common. The reaction of sulfuric acid with the carbonate host rock produces replacement gypsum and releases CO_2 (e.g., Hill, 2000; Hose, 2013; Palmer, 2013; Klimchouk, 2019; Palmer & Hill, 2019; De Waele et al., 2016, 2024).

The most frequently cited source of H_2S in SAS is the reduction of calcium sulfate within evaporite basins. The formation of several major caves around the world has been largely attributed to dissolution by sulfuric acid derived from nearby gypsum or anhydrite deposits. For example, calcium sulfate reduction within evaporite basins, along with hydrocarbons in these basins, has been identified as the source of hydrogen sulfide that contributed to the formation of famous caves such as Carlsbad Cavern and Lechuguilla Cave in the Guadalupe Mountains, New Mexico and Texas, USA (Hill, 1995, 2000; Palmer & Palmer, 2012; Palmer & Hill, 2019), Frasassi caves in central Italy (Galdenzi & Maruoka, 2003), and the Kane Caves in Wyoming, USA (Egemeier, 1981).

Another potential source of H_2S, independent of sulfate reduction, is mantle degassing (magmatic). This type of hypogene H_2S is typical in areas with volcanic activity or where deep active magma bodies are located (De Waele & Gutiérrez, 2022; De Waele et al., 2024).

The reaction of sulfuric acid with carbonate rocks, including travertine, results in the formation of large and thick gypsum deposits on the cave floor (e.g., Galdenzi & Maruoka, 2003; De Waele et al., 2016, 2024; De Waele & Gutiérrez, 2022). However, a significant contribution to their accumulation is the crystalline gypsum crusts that fall from the walls and ceiling. Thick wall rinds, up to 30 cm, are formed in

*andrzej.tyc@us.edu.pl

such caves due to condensation corrosion involving gaseous H_2S (Polyak & Provencio, 2001). The active process of carbonate wall replacement by gypsum is recorded from many SAS caves globally (e.g., Galdenzi & Maruoka, 2003; D'Angeli et al., 2019a, b; De Waele et al., 2016, 2024; Palmer & Hill, 2019).

The worldwide occurrence and general characteristics of sulfuric acid caves were recently summarized in a review article by De Waele et al. (2024). Active and non-active SAS caves are well documented, primarily in Europe and the USA. However, caves formed through sulfuric acid processes, or exhibiting manifestations of such processes, are found in different regions worldwide. The Peruvian Andes, due to its geodynamic position and evolutionary history, including widespread Late Miocene magmatism and intrusions into older carbonate sedimentary sequences, is a region with potentially numerous hypogene karst areas. Recent studies by Klimchouk et al. (2023) have documented examples of hypogene karst, though not specifically SAS, in the Peruvian high Andes. Evidence of sulfuric acid speleogenesis in the Andean range includes Brujas Cave in Argentina (see Forti et al., 1993; Sancho et al., 2002, 2004; De Waele et al., 2024). Forti et al. (1993) proposed that the cave's formation began with the upwelling of hydrogen sulfide fluids from an oil pool. However, sulfur isotopic analysis of gypsum deposits by Sancho et al. (2002, 2004) suggests a more complex origin of Brujas Cave, with a limited role of SAS.

The deposition of travertine can accompany the discharge of sulfur-rich thermal waters and is one of the manifestations of active sulfuric acid speleogenesis (Hose, 2013). Extensive travertine deposits associated with such processes are described from Sistema Zacatón in Mexico (Gary & Sharp, 2006, 2009). Hypogene caves in travertines can also be related to rising CO_2-rich thermal waters, such as documented in Mesa del Oro in New Mexico (Polyak et al., 2024). In the Mulapampa travertine in the Andes, evidence of SAS is found in a cave formed within a thick travertine cover.

Over the course of a multi-annual research project, we identified and explored three caves situated in collapse sinkholes within an extensive Pleistocene travertine formation in the Central Andes. Our main objective was to recognize the speleogenetic factors influencing these caves and discern their origin. Although we did not identify diagnostic morphological features typical of SAS caves, this article presents geochemical and mineralogical evidence suggesting possible SAS stage(s) in the karst evolution of the Mulapampa travertine. The research primarily focused on Gruta con Lago, whose lowermost part reaches the modern water table and hosts significant fine-grained gypsum deposits and replacement gypsum crusts on its walls. A notable indication of sulfuric acid activity in this cave is the isotopic composition of sulfur and oxygen of studied sulfates.

GEOGRAPHICAL AND GEOLOGICAL SETTING

The studied caves within the travertine deposits, locally known as the Mulapampa travertine, are situated in the central section of the Huambo River valley. This valley is a left-bank tributary of the Colca River (also referred to as the Camaná-Majes-Colca River), within the Colca River basin in the Western Cordillera of the Central Andes (Fig. 1A). The 40 km long Huambo River originates approximately at 4,400 m a.s.l. and joins the Colca River at 1,420 m a.s.l. Downstream of Huambo town, the river carves a deep canyon through Mesozoic sedimentary formations. Upstream, near the Mulapampa travertine, the river is typically dry for most of the year and only flows temporarily following the rainy season. Permanent flow is present below the main spring, Manco Cápac, located upstream of Huambo town (see H1 at Fig. 1B). The spring drains the main outcrop of the Mulapampa travertine. Notably, the travertine is characterized by numerous deep collapse sinkholes. Three of these sinkholes were explored and documented by the authors, and the caves within them are the focus of this article (C1-C3 in Fig. 1B).

The studied area is located on the western edge of the overriding plate (South American Plate), above the subducting Nazca plate (Fig. 1A). This geotectonic setting results in significant seismic activity including subduction earthquakes (e.g., Benavente et al., 2017; Gaidzik & Więsek, 2021; Woszczycka et al., 2024), and related mass movement processes (e.g., Gaidzik et al., 2020; Delgado et al., 2022), volcanic activity manifested by recent eruptions (e.g., Samaniego et al., 2016; Boixart et al., 2020; Machacca et al., 2023), as well as geysers and thermal springs (e.g., Ciesielczuk et al., 2013; Tyc et al., 2022).

The Upper Jurassic-Cretaceous sedimentary rocks of the Yura (quartzite, sandstone, and mudstone), Murco (sandstone and mudstone), Arcurquina (limestone with cherts), and Ashua Formations (limestone, sandstone, mudstone and evaporites – gypsum and salt) are the oldest formations exposed in the studied section of the Huambo River deposits (Fig. 1B; Caldas, 1993; Romero Fernández & Ticona Turpo, 2003; Paulo et al., 2013). These sedimentary formations are intruded by the Upper Cretaceous-Eocene dacite bodies with contact alterations in the sedimentary deposits (Paulo et al., 2013). The Pleistocene-Holocene Mulapampa travertine cover lies directly and unconformably on Mesozoic sedimentary formations, showing no apparent contact with dacite intrusions. Beneath the travertines, there is a thick (500-700 m) sequence of carbonate rocks from the Arcurquina Formation. On the periphery, the travertines are covered with Quaternary colluvial and alluvial deposits (Fig. 1B). Lavas from the Pleistocene-Holocene Andahua Group are also reported in this area; however, their spatial and temporal relationship with the travertine deposits remains unknown (Fig. 1B). These lavas are primarily composed of trachyandesites, basaltic trachyandesites, trachytes and dacites (Sørensen & Holm, 2008; Gałaś, 2014).

A comprehensive study of the Mulapampa travertine has not been conducted thus far. Basic structural and geochemical information is derived from our own observations and analyses. The travertine extends over approximately 11 km^2 and can reach a

considerable thickness, locally exceeding 100 meters. These carbonate deposits occupy the central part of the Huambo River valley (Fig. 1B). They extend from an elevation of 2,970 m a.s.l. in the NNW part downstream of the Huambo town to ca. 3,950 m a.s.l. in the SSE part. The eastern peripheries, which are adjacent to slopes and covered with colluvial deposits, reach elevations of up to 4,000 m a.s.l. (Fig. 1).

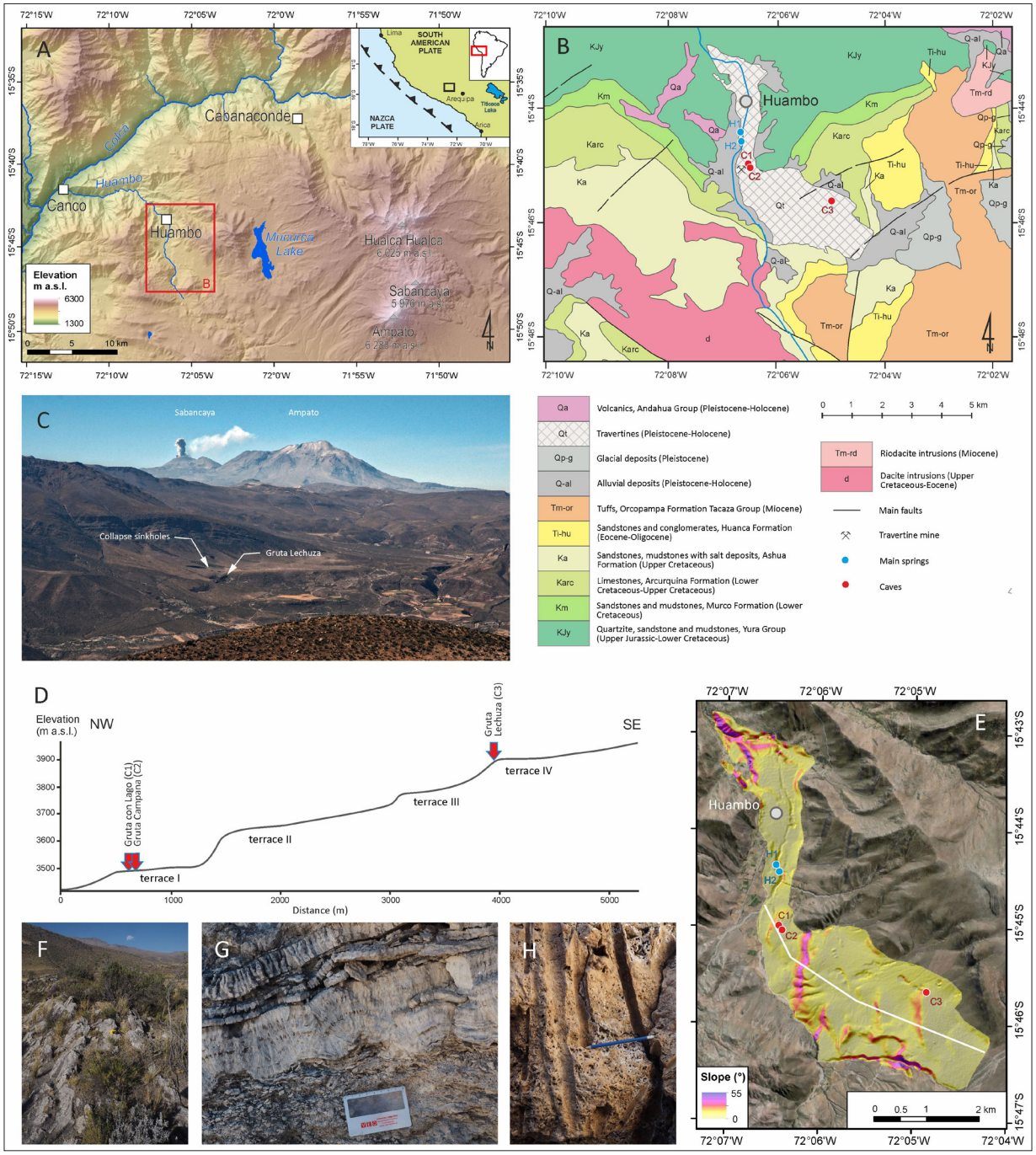

Fig. 1. Location of the study area. A: general location of the Mulapampa travertine and studied caves in the central Colca River basin (shaded relief map based on 30 m resolution digital elevation model, DEM from Shuttle Radar Topography Mission, SRTM https://earthexplorer.usgs.gov); B: Geological settings of the Mulapampa travertine (based on Caldas, 1993 and Romero Fernández & Ticona Turpo, 2003, modified) with location of the studied caves (Gruta con Lago – C1, Gruta Campana – C2, Gruta Lechuza – C3) and springs (Manco Cápac Spring – H1 and upper spring in Huambo – H2); C: Upper terraces of Mulapampa travertine overlooking the Ampato-Sabancaya Volcanic Complex (ASVC), with active Sabancaya volcano (view from NW); D: Morphological profile through the Mulapampa travertine complex (profile line shown in Fig. 1E – white line); E: Location of studied caves and springs on the Mulapampa travertine slope map (D and E based on 15 m resolution DEM; Esri, Maxar, GeoEye, Earthstar Geographics, CNES/Airbus DS, USDA, USGS, AeroGRID, IGN and the GIS User Community); F: Fissure ridge-like structure on the highest (IV) terrace of the travertine complex; G: Laminated crust with layers of ray-crystal columns; H: Paludal travertine with cylindrical voids, casts of reed stems.

The majority of travertine is exposed upstream of the Manco Cápac spring (H1 in Fig. 1B), forming at least four distinctive terraces separated by steep scarps up to 100 m high (Fig. 1D and E). These terraces are generally flat, with slopes not exceeding 5°. The lowest terrace is located in the central part of the Mulapampa travertine, south of the Manco Cápac Spring (Fig. 1B and E), at elevations between 3,443 and 3,463 m a.s.l. Moving SE, the surface of the travertine cover rises, with additional terraces occuring at elevations of 3,590-3,690 m a.s.l., 3,730-3,780 m a.s.l., and above 3,860 m a.s.l. Two of the studied caves, i.e., Gruta con Lago and Gruta Campana (C1 and C2 in Fig. 1B and E), are located on the lowest terrace (I in Fig. 1D).

The entrance to the third cave, Gruta Lechuza (C3 in Fig. 1B and E), is situated at the edge of the highest terrace (IV in Fig. 1D).

The travertine surfaces are mostly covered with semi-arid vegetation and are exposed in erosion or road cuts and on the walls of collapse sinkholes and caves. Given their location in a tectonic and volcanic zone active throughout the Pleistocene and Holocene (Samaniego et al., 2016; Benavente et al., 2017), the spatial morphological diversity and observed facies, the Mulapampa travertine can be classified as thermogene (according to Pentecost & Viles, 1994; Pentecost, 2005). This travertine exhibits a subhorizontal to gently dipping (up to 10°) bedded succession, predominantly composed of crust facies. These facies include alternations of several-centimeter-thick abiotic crystalline crusts, characterized by feather-like and ray-crystals (Fig. 1G). Horizons of rapid deposition around the stems of grasses and reeds in a paludal environment can also be identified within the travertine succession (Fig. 1H). Moreover, on the highest terrace, there are well-developed fissure ridge structures (Fig. 1F). Locally, the travertine layers are intercalated with colluvial sediments with calcareous cement.

The climate of the Colca River basin is generally temperate and dry, with seasonal rains occuring from December to March-April, and significant variations in temperature and precipitation depending on the elevation a.s.l. (Zavala et al., 2014; Tyc et al., 2022). Within the Colca River basin, which spans between elevations 1,200 to over 6,000 m a.s.l., the Huambo area – where the Mulapampa travertine and studied caves are located – lies in medium elevations (2,800-4,000 m a.s.l.). This results in the mean annual temperature ranging between 6.5 and 17.6°C, and annual precipitation varying from 150 to 600 mm (Zavala et al., 2014). Data from the meteorological station located in Huambo at 3,312 m a.s.l., corroborate these general values (https://www.senamhi.gob.pe). For the years 2022-2023, the mean maximum recorded temperature was approximately 19.2°C, ranging from around 13 in December and March to over 25°C in July and October. The mean minimum temperature ranged from below 0°C in June and August, to above 7°C from December to March, with a mean annual minimum temperature of 3.9°C. The annual precipitation recorded in Huambo station is about 400 mm, predominantly falling between December and early April. Occasionally, particularly in February, the daily precipitation can reach up to 50 mm.

METHODS AND MATERIALS

Field studies

Fieldwork in the area of Mulapampa travertine was conducted during three field campaigns: in September 2017 as part of the Polish Scientific Expedition to Peru, and in June 2022 and June/July 2023 as part of a research project funded by the National Science Centre of Poland. Three caves developed in travertine were identified and explored in 2017: Gruta con Lago, Gruta Campana, and Gruta Lechuza (see Fig. 1 for location). After consultation with the local community, the authors proposed the cave names used in this article. During the 2022 and 2023 expeditions, the caves were surveyed, and extensive photographic documentation was conducted. Cave surveys were done using a DistoX measuring device. Samples of travertine from the surface outcrops, as well as mineral precipitates and sediments, and the waters found in Gruta con Lago were collected. For comparison, water samples were also taken from two springs located below the identified caves. Location of water sampling sites are indicated in Figures 1 and 2. In 2022, an air temperature and humidity logger was installed in the Gruta con Lago.

Water samples were collected during the dry season to reduce dilution with meteoric waters. Physical parameters, including water temperature, pH, electrical conductivity and redox potential were measured in the field using a multifunction portable pH/conductivity meter CPC-411 equipped with a temperature sensor, offering an accuracy of ±0.1°C, ±0.01 pH, ±0.25% of conductivity and ±1 mV, respectively.

Water samples from Gruta con Lago and springs were collected using two high-density polyethene bottles and filtered in the field through a 0.45 µm membrane filter. Samples for the analysis of cations and dissolved metals were acidified with ultra-pure HNO_3. Unacidified samples were utilized for anion and the isotopic analysis. Samples for oxygen and hydrogen isotope analysis were collected duplicative in 5 ml glass vials.

For monitoring air temperature and relative humidity within the Gruta con Lago Cave, a HOBO U23 Pro v2 data logger from Onset was used. The device is equipped with built-in temperature and relative humidity sensors. The temperature sensor has a measuring accuracy of ±0.21°C (within the temperature range of 0-50°C) and a resolution of 0.001°C, while the relative humidity sensor has an accuracy of ±2.5% (within the RH range of 10-90%) reaching a maximum of ±3.5% including hysteresis at 25°C. Below 10% and above 90%, the accuracy is ±5%. The data was recorded at 30-minute intervals. This article used data from June 10, 2022, to June 30, 2023. For comparison, meteorological data were used - maximum and minimum daily temperature and daily rainfall, from the station in Huambo belonging to the National Service of Meteorology and Hydrology of Peru (Servicio Nacional de Meteorología e Hidrología del Perú; https://www.senamhi.gob.pe).

Laboratory methods

Chemical analyses of water samples were performed at the Hydrogeochemical Laboratory of the AGH University of Krakow, Poland. Filtrated and acidified samples were analyzed using inductively coupled plasma optical emission spectrometry (ICP-OES) and inductively coupled plasma mass spectrometry (ICP-MS) using Optima 7300DV (PerkinElmer, Waltham, MA, USA) and iCAP RQ (C2) (Thermo Fischer Scientific, Waltham, MA, USA) spectrometers, respectively. The B, Ba, Ca, K, Li, Mg, Mn, Na, Si, and Sr concentrations were determined using the ICP-OES technique. The

TraceCERT® (Sigma-Aldrich, Saint Louis, MO, USA) single- and multi-element standard solutions were used for instrument calibration. Unfiltered and unacidified samples were used for chloride and bicarbonate determination. For this reason, the titration methods were applied according to the appropriate ISO standards. Certified reference materials TMDA 64.3 and TM 23.5 (Environment and Climate Change Canada) and Hard Drinking Water UK – Metals (LGS Standards Ltd., UK) were used for quality control.

Saturation indices were calculated using the PHREEQC version 3 software, and graphs were prepared in the PS IMAGO PRO software package (with the IBM SPSS Statistics analytical engine).

The isotopic analysis of water samples ($\delta^{18}O$ and $\delta^{2}H$) was performed in the Institute of Earth and Environmental Sciences laboratory, Maria Curie-Sklodowska University in Lublin, Poland. The $\delta^{18}O$ and $\delta^{2}H$ values were determined on a Picarro L2130-i Analyzer using the method of Cavity Ring-Down Spectroscopy. The water samples were analyzed automatically along with two IAEA standards, VSMOW 2 ($\delta^{18}O$ = 0.0‰, $\delta^{2}H$ = 0.0‰) and GRESP ($\delta^{18}O$ = -33.4‰, $\delta^{2}H$ = -258.0‰), during each measurement session, one internal standard is also measured. The analytical precision (1σ) and reproducibility were generally better than 0.1‰ and 1‰ for $\delta^{18}O$ and $\delta^{2}H$, respectively.

Analyses of the isotopic composition of sulfur ($\delta^{34}S$) and oxygen ($\delta^{18}O$) in gypsum samples, and sulfate ions in cave and spring water were performed in the Stable Isotopes Laboratory, Institute of Geological Sciences of the Polish Academy of Sciences in Warsaw, Poland. The Flash EA 1112HT elemental analyzer (Thermo Scientific) coupled to a Delta V Advantage Mass Spectrometer (Thermo Scientific) in a continuous He flow system was used for analyses of both isotopes. The high temperature conversion method was used for $\delta^{18}O$ measurement, while for $\delta^{34}S$ determination, the dynamic combustion method was used. Dissolved sulfates from water samples were precipitated with $BaCl_2$ to $BaSO_4$ for isotopic analysis of $\delta^{34}S$ and $\delta^{18}O$. Gypsum samples were dissolved in deionized water acidified by adding HCl and then precipitated as $BaSO_4$ by adding barium chloride. Measurements were calibrated using international standards NBS 127, IAEA SO-5, and IAEA SO-6. Two subsamples were taken from each sample. The measurement results were given for $\delta^{18}O$ vs. VSMOW and $\delta^{34}S$ vs. VCDT. The analytical precision (1σ) was ±0.3‰ for $\delta^{34}S$ and ±0.5‰ for $\delta^{18}O$.

Samples of carbonates (travertine) from surface outcrops and from Gruta con Lago, and mineral deposits (sulfates) from the cave were examined at the Institute of Earth Sciences, the University of Silesia in Katowice, Poland. Qualitative chemical composition and mineral habits were investigated using a Philips XL 30 ESEM/TMP scanning electron microscope coupled with an energy-dispersive spectrometer (EDS; EDAX type Sapphire). The phase composition of mineral samples from caves was established by X-ray diffraction (XRD). This work involved a Philips PW 3710 diffractometer. Diffraction patterns were interpreted using the X'Pert HIGHScore Plus software.

RESULTS

Caves of the Mulapampa travertine

The distinctive feature in the surface morphology of the Mulapampa travertine is the presence of numerous deep collapse sinkholes. Three caves were identified during field studies focused on the spatial distribution and origin of these sinkholes. These caves were already known to the local community in Huambo. Evidence of past human activity in the vicinity of two of these caves includes remains of old artificial stone structures found within the collapse sinkhole walls and bottom.

Entrances of Gruta con Lago and Gruta Campana (C1 and C2 in Fig. 1B and E) are situated on a gently sloping travertine terrace (I in Fig. 1D) at elevations of 3,447 and 3,463 m a.s.l., respectively. Both caves are characterized by deep, cylindrical or bell-shaped collapse sinkholes. From the bottom of these sinkholes, steep cones of collapsed travertine blocks lead to the cave floors.

The sinkhole collapse entrance of Gruta Campana is round with a diameter of 11 m (Supplementary Fig. S1A) and has a depth of 29 m. The cave continues steeply downward towards the east through a tight passage between wedged travertine blocks. The cave floor, covered with clastic sediments washed in from the surface, is approximately 40 m deep (Supplementary Fig. S1B). This part of the cave shows signs of frequent surface water flow and likely experiences periodic flooding during the rainy season. To the northwest, a nearly horizontal passage extends between large travertine blocks and intact travertine surfaces, at a depth of about 30-35 m below the surface. This area contains remnants of gypsum replacement crusts (Supplementary Fig. S1C).

The collapse sinkhole of the Gruta con Lago is elliptical, with a long axis (N-S) of 35 m and a short one (W-E) of 25 m (Fig. 2A and B). The bottom of this sinkhole, covered with travertine blocks and overgrown by bushes and trees, is at a depth of 15 m. In the southern part, a steep cone of travertine blocks descends to the cave floor (Fig. 2C). At the bottom of the cave, located at a depth of 38 m below ground level, there is a small lake and several smaller water pools formed between the collapsed blocks and mass of gypsum deposits. The underground water flow is accessible in two places at the cave bottom. In a side passage developed along the NE-SW direction, underground flow is accessible in two other places (Fig. 2A). This study focuses primarily on the Gruta con Lago because of the presence of the water table and of mineralogical and geochemical features potentially associated with sulfuric acid speleogenesis.

The giant collapse sinkholes in the Mulapampa travertine are located on the uppermost travertine terrace (IV in Figure 1D), which is partly covered by colluvium. The deepest known cave in the studied area, Gruta Lechuza, is located on the edge of this terrace. The cave entrance is situated in the SE part of a large, elongated collapse sinkhole, which measures 200 m along its longer axis (NW-SE) and 85 m along its shorter axis (NE-SW) (see C3 in Fig. 1B;

Supplementary Fig. S2A and C). The maximum depth of the sinkhole is approximately 35 m, while the the cave bottom is almost 85 m below ground level, at the elevation of 3,771 m a.s.l.

The entrance to the cave (Supplementary Fig. S2B) features a strongly inclined cone of collapsed blocks (Supplementary Fig. S2D), leading to a vertical wall and a zone of large travertine blocks mixed with layers of sharp-edged colluvium (approximately 70 m below the ground surface). This section of the cave also contains solution features, including small cupolas in the ceiling (Supplementary Fig. S2G). Some solution forms, primarily anastomosing channels, are filled with fine-grained clastic sediments, which also accumulate in the lowest parts of the cave (Supplementary Fig. S2F). Historically and currently, mud and debris from the steep slopes surrounding the travertine terrace to the east are transported into the cave, contributing to sediment accumulation. A high-energy water and mud flow event in February 2023 interrupted the recording of microclimatic parameters within the cave. Gypsum deposits are present in the side cracks and on the cave floor (Supplementary Fig. S2F).

The caves in the Mulapampa travertine are notable for their depth. Reaching up to approximately 85 m, they rank among the deepest travertine caves in the world. The deepest known travertine cave, Zendan-e Soleyman in Iran, is reported to be 109 m deep (Damm, 1968) or around 80 m according to modern UNESCO (2024) data (https://whc.unesco.org). Zendan-e Soleyman is classified as a primary, constructional travertine cave (Gradziński et al., 2018).

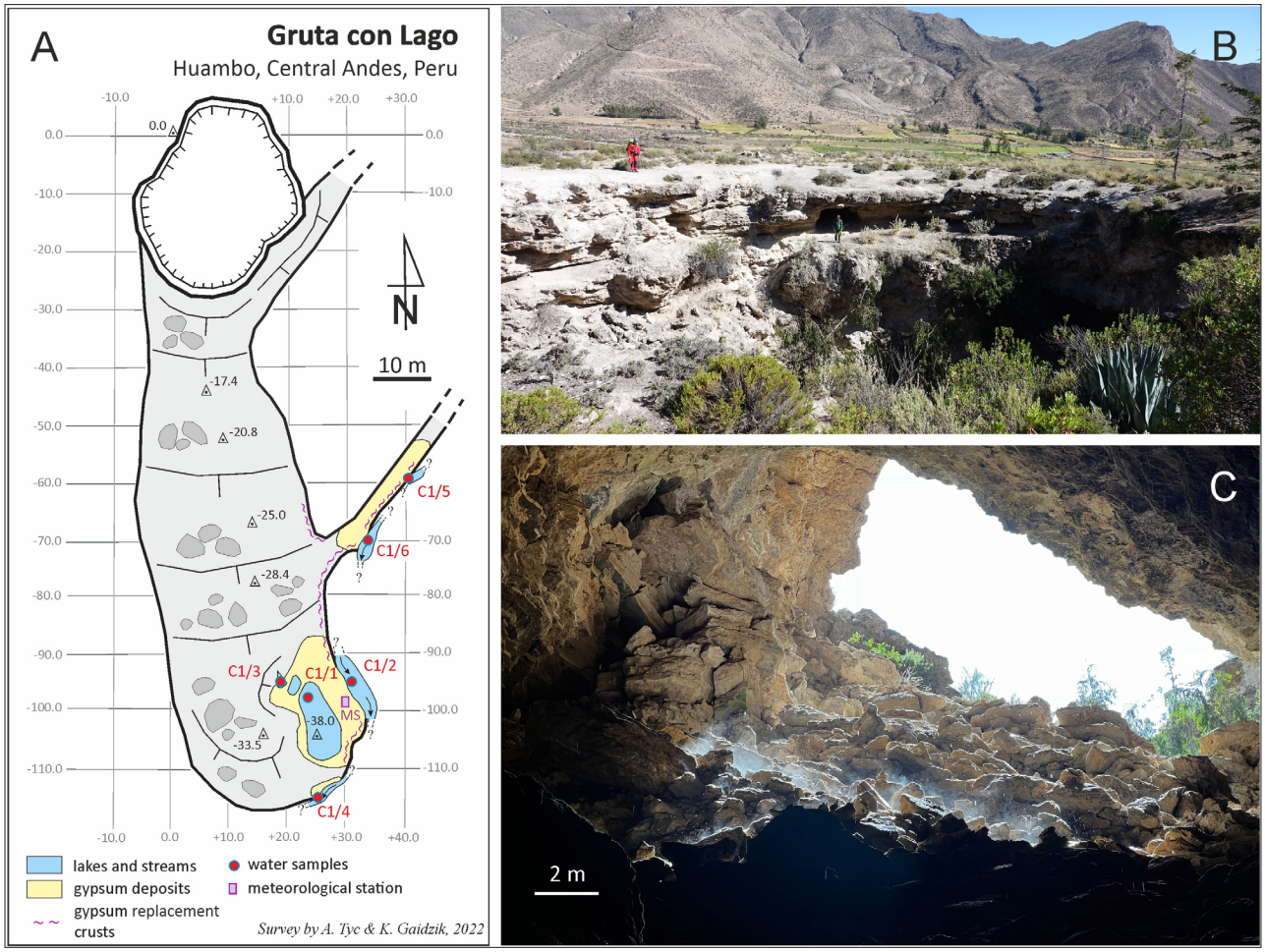

Fig. 2. Gruta con Lago. A: Cave survey with location of gypsum deposits and crusts, and location of water samples (see Table S1); B: Collapse sinkhole forming the cave entrance; C: Collapsed travertine strata and talus of breakdown travertine blocks.

Environmental conditions in Gruta con Lago

Gruta con Lago exhibits specific environmental conditions, shaped by its northern-facing entrance, the steeply inclined cone formed by collapsed travertine blocks, and the cave floor positioned at the water table (Fig. 2). A key factor in the preservation of substantial gypsum deposits and the ongoing degassing of H_2S is the cave's isolation from external geomorphological processes.

The cave interior receives sunlight (Fig. 3A, B), causing daily fluctuations of microclimatic parameters and promoting algae growth on some of the collapsed travertine blocks. Despite its high-altitude location, the air temperature in the cave remains above freezing year-round. Based on one year of air temperature monitoring (from June 10, 2022, to June 30, 2023), the average temperature was 7.4°C, with a maximum of 10.5°C in April and a minimum of 4.2°C in June. The average humidity was 92.9%, peaking at 100% during the rainy season (December to April) and dropping to a minimum of 61.5% in June (Fig. 3C, D).

Water chemistry at Gruta con Lago and in Huambo springs

The physicochemical characteristics, chemical, and isotopic composition of the water from the Gruta con Lago and springs draining the travertine massive are summarized in Supplementary Table

S1. General chemical composition (major ions) is shown in the Piper diagram (Fig. 4A). The water temperature measured in the cave ranges from 15.6-15.8°C at site C1/3 (see Figure 2A and 7C) to 16.5-16.7°C at site C1/4 (see Figure 2A and 5E). The water in the underground stream flowing through the cave is slightly warmer (0.5-0.9°C). The Manco Cápac Spring (H1 in Supplementary Table S1; Fig. 1B and 7F) in the Huambo River Valley shows a water temperature similar to the one flowing in the cave (16.6-17.1°C). In comparison, the H2 spring located several dozen meters upstream in the valley has a temperature 16.1°C, similar to that in the stagnant waters in the cave (C1 in Supplementary Table S1). The temperature of both the water in the cave and in the spring is higher than the average annual air temperature at this elevation in the Huambo area. Despite this, they should be classified as cold waters within the geothermal region of the Colca River basin (Tyc et al., 2022).

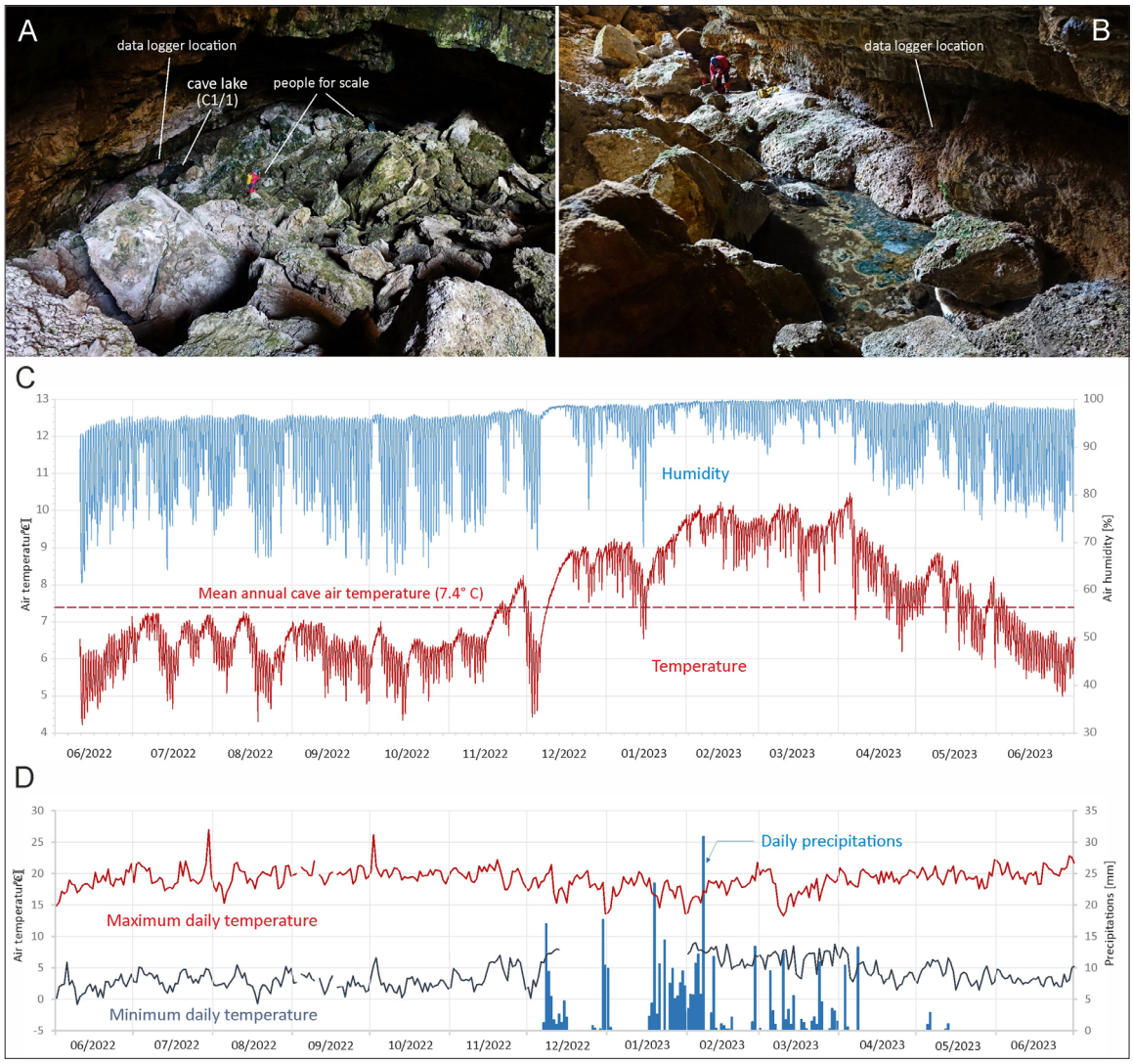

Fig. 3. Environmental conditions in the Gruta con Lago. A: Algae growing on the travertine collapse blocks (view from the entrance); B: Lake and zone of gypsum deposits at the bottom of the cave (view towards the entrance); C: Annual changes in the air temperature and relative humidity at the bottom of the cave (the logger is placed out of sunlight); D: Annual changes in maximum and minimum air temperature and daily precipitations at the meteorological station in Huambo (after https://www.senamhi.gob.pe).

The pH values of the water in the lake and flowing in the cave are within a narrow range of 6.51-6.90, except for one measurement at site C1/6, where a pH of 5.30 was recorded (Supplementary Table S1). More neutral to alkaline waters flow out through springs (pH 6.63-7.15). The generally positive (oxidizing conditions) redox potential in the cave waters and springs is negative (reductive conditions) only at site C1/3 (-28 to -130 mV; see Supplementary Table S1). This was also the only site where a gentle outgassing and faint smell of H_2S was detected (see Fig. 5C and D).

All studied waters belong to the bicarbonate-rich hydrochemical group (Fig. 4A) and are of Ca-HCO_3-SO_4 type. Bicarbonates dominate their chemical composition (351-626 mg/L in the cave and 386-588 mg/L in springs). Sulfates are the second most significant component (254-374 mg/L). Temporal variability of the content of these ions is observed, but it is more pronounced in cave waters. Calcium content varies from 197 to 257 mg/L and magnesium from 24.2 to 42.4 mg/L. The total dissolved solids (TDS) for all water samples are within the 0.9-1.3 g/L range (Supplementary Table S1).

The waters in the Mulapampa travertine exhibit properties similar to the bicarbonate-rich cold and thermal waters from the springs located on the slopes of the extinct Hualca-Hualca Volcano (Fig. 4). The Huambo Spring (H2) studied in 2017 (Tyc et al., 2022) had waters with properties of sulfate-rich cold waters (Fig. 4A).

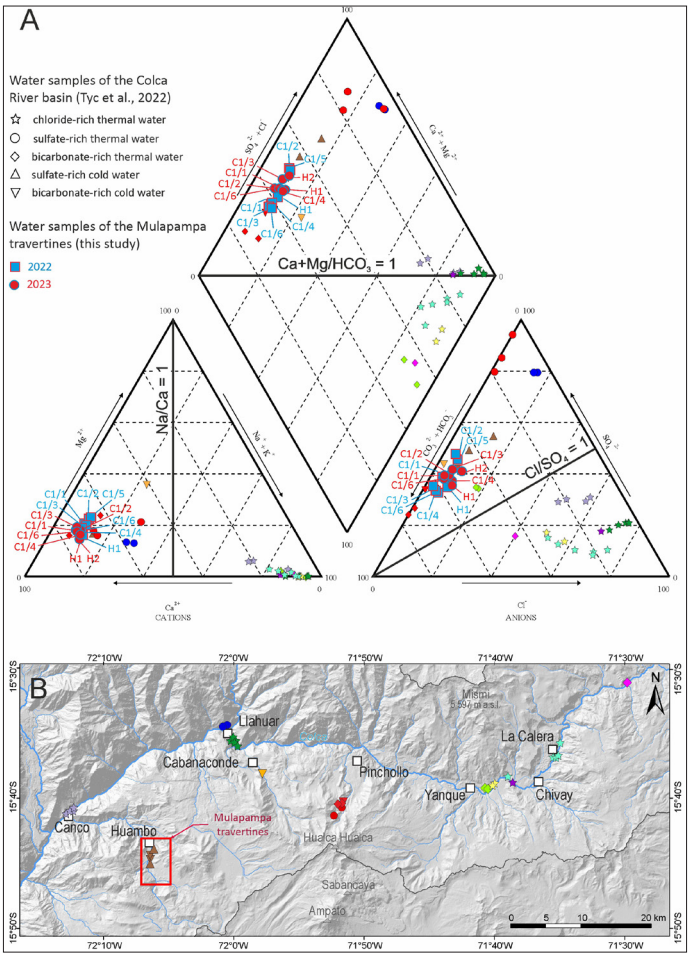

Fig. 4. A: Piper diagram showing the chemical composition of water samples from Gruta con Lago and springs near Huambo against the background of the chemical composition of cold and thermal waters of the central Colca River basin (based on Tyc et al., 2022). B: Map of the spatial distribution of compared springs and geysers (modified after Tyc et al., 2022).

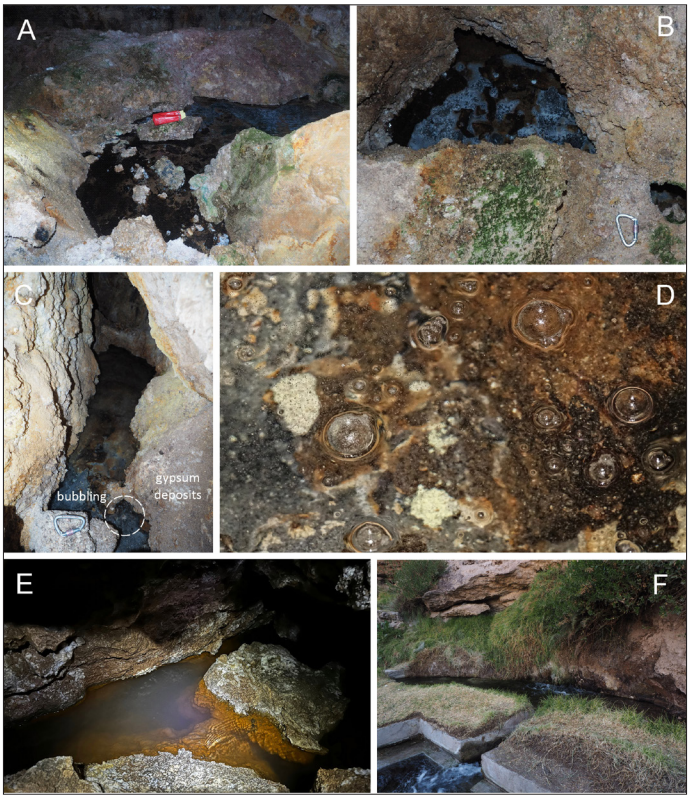

Fig. 5. Small lakes and underground streams in the Gruta con Lago (A – E) and the Manco Cápac Spring (F). A: Small lake at the cave bottom surrounded by thick gypsum deposits – site of water sample C1/1 on Fig. 2A; B: Small opening in the gypsum deposits filled with water – visible subaqueous white bacterial mats; C: Fracture between collapsed blocks of travertine covered with gypsum deposits and secondary sulfate crust and filled with stagnant water – the gentle outgassing zone is circled and enlarged in D (C1/3 on Fig. 2A); E: Underground flow at the lowest point of the cave (C1/4 on Fig. 2A); F: Manco Cápac Spring (H1 on Fig. 1B).

The studied waters from Gruta con Lago and springs are characterized by high strontium content, ranging from 2.44 to 2.63 mg/L (Supplementary Fig. S3). Significant concentrations of boron (340-600 µg/L), manganese (5-219 µg/L), lithium (30-40 µg/L) and barium (26-35 µg/L) are also recorded (Supplementary Table S1). Although most trace elements show little variation over time and space, manganese concentrations vary significantly. The highest manganese content was detected at the downstream section of the underground flow in Gruta con Lago (C1/4; see Fig. 2A), while the lowest was found in the Manco Cápac Spring (H1; Fig. 1B).

Two series of analyses (in 2022 and 2023) allowed us to assess the aggressiveness of the waters in relation to calcite and gypsum in the Gruta con Lago and the springs. The calcite saturation index indicates that all analyzed waters are in equilibrium with respect to calcite (Fig. 6A; Supplementary Table S1). However, localized supersaturation is possible, as evidenced by the calcite rafts observed on the surface of stagnant cave waters in 2022 (sites C1/3 and C1/5). In contrast, all studied waters are aggressive toward gypsum (Fig. 6B; Supplementary Table S1).

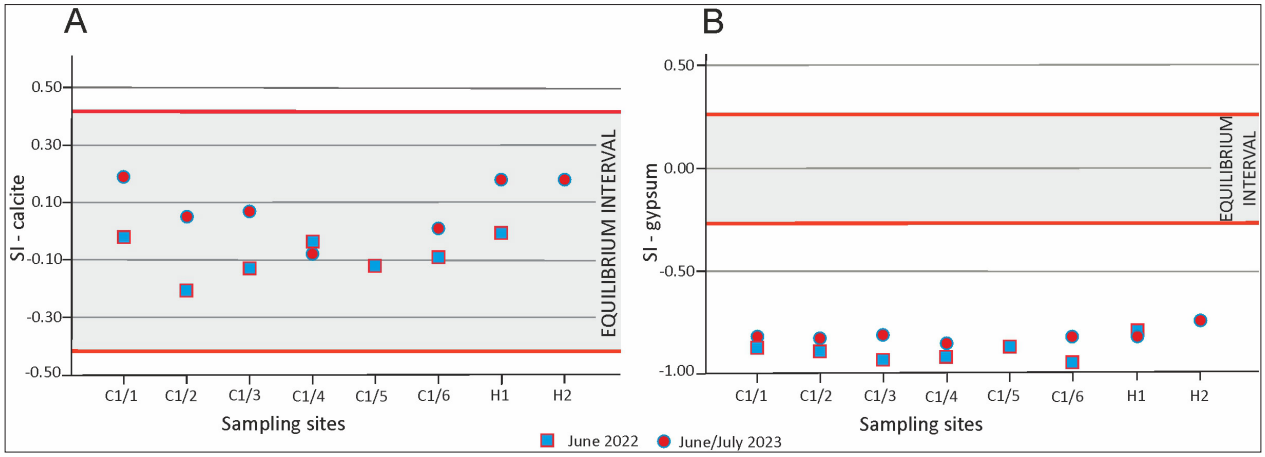

Fig. 6. Saturation indices of calcite (A) and gypsum (B) in waters from the Gruta con Lago (C1/1 – C1/6) and from springs (H1, H2) (data available in Supplementary Table S1); equilibrium interval for both indices was modelled by PHREEQC.

Mineral deposits in Gruta con Lago

The presence of gypsum in the Gruta con Lago, and to a less extent in Gruta Campana, prompted us to explore its potential link to the role of H_2S in the speleogenesis of the Mulapampa travertine caves. Significant gypsum deposits and crusts are primarily concentrated in the eastern part of the Gruta con Lago and within its side passage (Fig. 2A), with no occurrences in the rest of the cave. The gypsum appears in various forms: (1) massive accumulation on the cave floor, (2) replacement crusts on the cave walls, and (3) crystals that have precipitated on these crusts due to evaporation (Fig. 7A-F).

The massive floor accumulations largely result from the detachment and falling of gypsum rinds from the cave walls. The thickness of gypsum and the associated insoluble residue reaches several dozen centimeters, and in certain areas exceeds one meter. X-ray diffraction analysis of these deposits reveals variable gypsum contents, ranging from 76 to 99%.

Two distinct types of gypsum crusts are found on the cave walls. In the eastern section of the main part of the cave and in the side passage, there are gypsum replacement crusts (Fig. 7D, E), which are typically associated with condensation corrosion in presence of H_2SO_4. However, no replacement pockets were observed in these areas. In the side passage, near the C1/6 water sampling point (Fig. 3A), laminated gypsum crusts are found on horizontal or sub-horizontal surfaces of travertine. These crusts reflect the texture and surface characteristics of the adjacent bedrock, and resemble replacement subaqueous crusts of gypsum (according to Buck et al., 1994; Palmer & Palmer, 2004) (Fig. 7B).

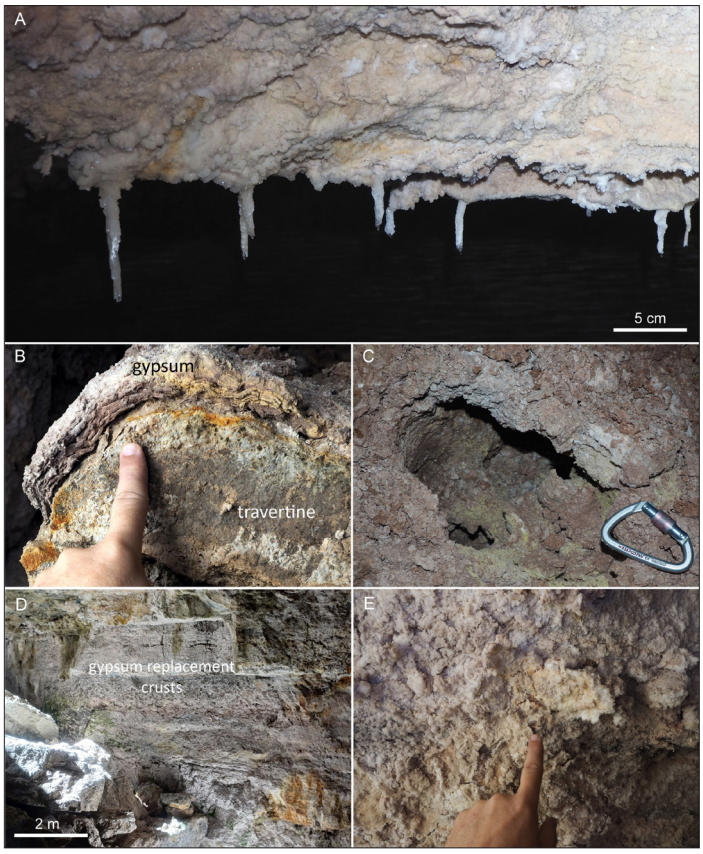

Fig. 7. Speleogenetic by-products in the Gruta con Lago Cave.
A: Evaporitic gypsum crystals precipitated on the gypsum crust covering the roof above the underground stream in a side passage (site C1/6; Fig. 2A); B: Transition between travertine and speleogenetic gypsum – volumetric replacement of travertine by gypsum in the side passage; C: Thick deposits of speleogenetic gypsum on the cave floor; D: Gypsum replacement crusts on the eastern wall of the cave and collapse blocks; E: Fragment of the cave wall covered by gypsum replacement crust.

Figure 8 shows microscopic images of gypsum deposits at the bottom of Gruta con Lago. The primary mass of sediment accumulating at the cave bottom consists of monoclinic gypsum crystal aggregates, with sizes ranging from several to over 100 µm (Fig. 8C-F). Among the massive gypsum accumulation, there are fragments of residual travertine (calcite crystals) which host tiny gypsum crystals on their surfaces (Fig. 8A and B). Additionally, tabular and needle-like crystals of celestine are commonly observed growing both on the cave floor gypsum and within the replacement crusts on the walls (Fig. 8). Barite is another secondary mineral identified in this cave.

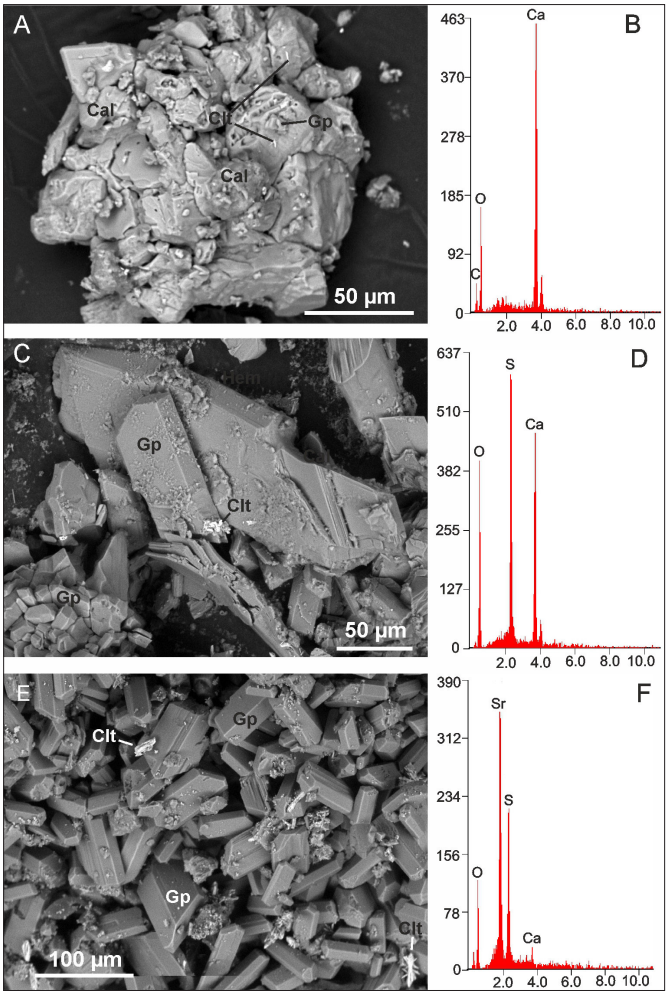

Fig. 8. SEM-BSE microphotographs of replacement gypsum in samples from gypsum deposits at the bottom of the Gruta con Lago. A: Residual calcite (Cal) with subordinate gypsum (Gp) and celestine Clt) crystals; C: Monoclinic gypsum crystals with tiny celestine; E: Tabular and needle crystals of celestine on gypsum; B, D, F: EDS spectrum of calcite, gypsum, and celestine.

DISCUSSION

When discussing the manifestations of SAS in the Mulapampa travertine, it is important to emphasize the lack of morphological (solutional) evidence of such speleogenesis in Gruta con Lago and the two other identified caves. The absence of characteristic replacement pockets on walls covered with replacement gypsum crusts may be due to the intense but relatively brief episode of sulfuric acid speleogenesis (SAS) in the Mulapampa travertine. The steepness of the cave walls likely also contributed, as it would facilitate the detachment and falling of the crusts. The basic morphology of all three caves is characterized by breakdown and block formation resulting from mechanical failure. The caves are open to the surface due to collapse. This poses a significant challenge in identifying the primary speleogenetic processes responsible for the formation of these voids, and, consequently, in confirming the role of SAS in the development of karst in the Mulapampa travertine. Due to the absence of morphological evidence in the studied caves, the focus has shifted to mineralogical and chemical signatures that indicate the former presence of sulfuric acid in the travertine massif.

Mineralogical evidence of sulfuric acid speleogenesis in Gruta con Lago

Minerals derived from the reaction between sulfuric acid and soluble host-rock (travertine and limestone in our case) is an essential manifestation of SAS (Polyak & Provencio, 2001; Galdenzi & Maruoka, 2003; Onac et al., 2009; De Waele et al., 2016, 2024). Such reaction gives rise to the formation of sulfate by-products. Gypsum, mostly as the wall rinds in form of crystalline crusts, is the most common by-product mineral of SAS (Hill, 1987; Polyak & Provencio, 2001; De Waele et al., 2024). It can precipitate or be deposit in the SAS caves in various forms, depending on conditions: subaerial or subaqueous (Buck et al., 1994; Polyak & Provencio, 2001).

A wide spectrum of gypsum forms occur in Gruta con Lago (Fig. 7). The eastern wall of this cave is covered by gypsum replacement crusts (Fig. 7D, E; see Fig. 2A for location), but no replacement pockets were found. There are also subaqueous replacement crusts covering the original travertine bedrock and blocks in a side passage (Fig. 7B). Almost the entire cave floor, outside the water, is covered by thick gypsum deposits (Fig. 7C).

Celestine, another sulfate mineral that can be considered a SAS by-product (Hill & Forti, 1997; D'Angeli et al., 2018), occurs commonly in Gruta con Lago. The waters of the geothermal system, enriched with Sr (see Supplementary Table S1 and Supplementary Fig. S3), could be the source of this metal. In combination with the presence of H_2S in the solutions, this may explain the occurrence of celestine in the cave.

Figure 9 shows the vertical and spatial distribution of the identified SAS mineralization occurrences. Based on this, it can be concluded that the zone of SAS manifestations is confined to the eastern part of Gruta con Lago and extends several meters above the current water table. This suggests that the processes responsible for the gypsum deposits and replacement crusts occurred relatively late, after the water table dropped, but most likely before the cave opened up to the surface.

The preservation of speleogenetic gypsum in Gruta con Lago is likely due to specific environmental factors, including the semi-arid climate of this part of the Andes and the microclimate within the cave itself (Fig. 3). Another important factor is the cave's isolation from modern geomorphological processes, such as mudflows and mud-debris flows, which affect the other two caves in the Mulapampa travertine almost every year.

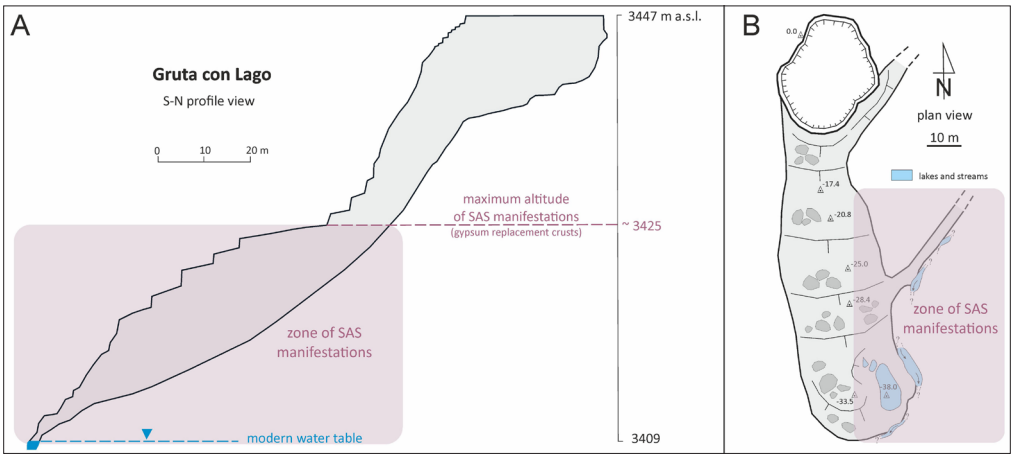

Fig. 9. Vertical extent (A) and spatial distribution (B) of SAS manifestations: sulfate mineralization in Gruta con Lago.

Sulfur and oxygen isotopic composition of mineral by-products

Chemical signatures indicating the former presence of sulfuric acid in currently inactive caves primarily involve sulfur stable isotopes found in the SAS by-products (Palmer & Hill, 2019; De Waele et al., 2024). Isotopic composition of sulfur alone is challenging to interpret (Onac et al., 2011; Temovski et al., 2018; Li et al., 2024), thus, recently, a combined investigation of both $\delta^{34}S$ and $\delta^{33}S$ (Laurent et al., 2023) and $\delta^{18}O$ in sulfates (e.g., Onac et al., 2011; Temovski et al., 2018; De Waele et al., 2024) was proposed. We used the analysis of both sulfur and oxygen stable isotope composition in sulfates and sulfate ions in water to identify the sulfur source and interpret the origin of sulfates. Although many factors control the oxygen isotopic composition of sulfate minerals, including ambient setting and type of sulfate-forming reactions, $\delta^{18}O$ values of sulfate can offer insights into the conditions prevailing during SAS (Onac et al., 2011; De Waele et al., 2024).

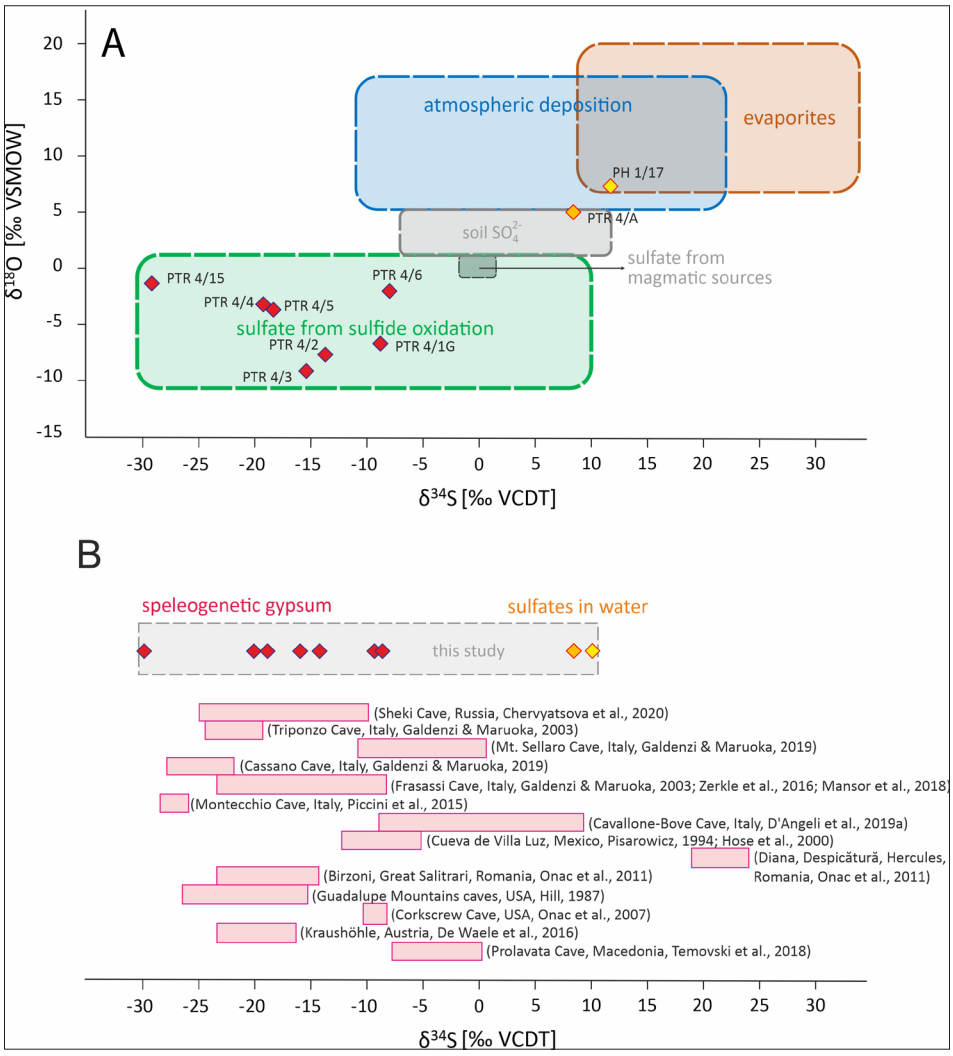

Fig. 10. Sulfur and oxygen isotopic composition of sulfur-containing minerals in the Gruta con Lago and sulfate ion in the cave lake and spring water (sample codes explained in Supplementary Table S2). A – $\delta^{34}S$ and $\delta^{18}O$ values of studied sulfates compared to typical ranges for different sulfur sources (based on Mayer, 2005; colored fields); B – $\delta^{34}S$ values of studied sulfates compared to literature data (based on Chervyatsova et al., 2020, modified).

Gypsum samples from the cave display a negative isotopic composition of sulfur and oxygen. In general, the cave gypsum shows a wide range of sulfur stable isotope values (from -19.4 to -8.2‰) and oxygen (from -9.0 to -1.3‰) (Fig. 10A and Supplementary Table S2). The soft sediment covered with microbial mat taken from the cave's lake bottom shows the lowest sulfur isotopic composition ($\delta^{34}S$ = -29.4‰). Low $\delta^{34}S$ values of various gypsum forms from the Gruta con Lago suggests their origin due to sulfide (H_2S) oxidation. This supports the hypothesis regarding the speleogenetic origin of gypsum deposits and crusts and that they are signature of subaqueous and/or subaerial oxidation of H_2S, followed by its oxidation to H_2SO_4 and reaction with travertine. The combination of sulfur and oxygen isotopic composition of sulfur-containing minerals from the Gruta con Lago compared to their characteristic ranges for different sulfur sources (after Mayer, 2005) is shown in Figure 10A. The results obtained for the studied cave are compared with the results of the sulfur isotopic composition of selected SAS caves worldwide (Fig. 10B). The summary is based on data presented in Chervyatsova et al. (2020).

The heavy isotopic composition of both sulfur and oxygen in water from cave's lake and Manco Cápac Spring (PTR4/A and PH1/17 in Table S2; Fig. 10A) indicate different sources of this sulfur. However, neither our studies nor the available regional literature provide isotopic reference values that enable us to determine the source of the sulfates dissolved in the waters of the travertine massif.

Geochemistry and stable isotopes of waters

The Mulapampa travertines are located in the Colca River basin geothermal system, which implies specific geochemical conditions of the waters circulating in this region. Processes controlling water chemistry are related to the location of the magmatic chamber of the Ampato-Sabancaya Volcanic Complex (ASVC) and tectonic structures that allow complex interactions of meteoric waters with the geothermal reservoir and spatial differentiation of thermal water types in that area. However, it should be emphasized that the geochemistry of the waters found in the Gruta con Lago and the Huambo springs are distinctly different from those in the thermal springs related to the geothermal system. The geochemical properties of cave and spring waters are slightly similar to bicarbonate- and sulfate-rich cold waters discharging on the periphery of the ASVC. Sulfate-rich thermal springs fed by meteoric water heated by ascending volatiles (including H_2S and CO_2) are active in the surrounding area (Fig. 4; Tyc et al., 2022).

In contrast to the central and eastern parts of the geothermal system, a complex of Mesozoic sedimentary rocks occurs in the Mulapampa travertine sector. There is a several-hundred-meter package of carbonate and siliciclastic rocks from the Arcurquina and Ashua Formations in the geological profile above the magma chamber. This factor substantially determines the geochemistry, including the composition of stable isotopes of the waters in Gruta con Lago and Huambo springs.

Isotopic water composition in Gruta con Lago shows general similarity between all studied sites and between two sampling campaigns. $\delta^{18}O$ of these waters is in the range of -14.8 to -15.6‰ and $\delta^{2}H$ in the range of -118 to -121‰ (Supplementary Table S1). Cave and spring waters have a negative hydrogen shift with respect to the Local Meteoric Water Line (LMWL; for northern Chile, after Boschetti et al., 2019; Valdivielso et al., 2021) and the Global Meteoric Water Line (GMWL; after Craig, 1961, modified by Rozanski et al., 1993) (-6.9 to -9.7‰ and -10.1 to -13.0‰, respectively; Fig. 11). $\delta^{18}O$ values of these waters are slightly more positive with respect to both, GMWL and LMWL (0.8 to 1.2‰ and 1.3 to 1.6‰, respectively).

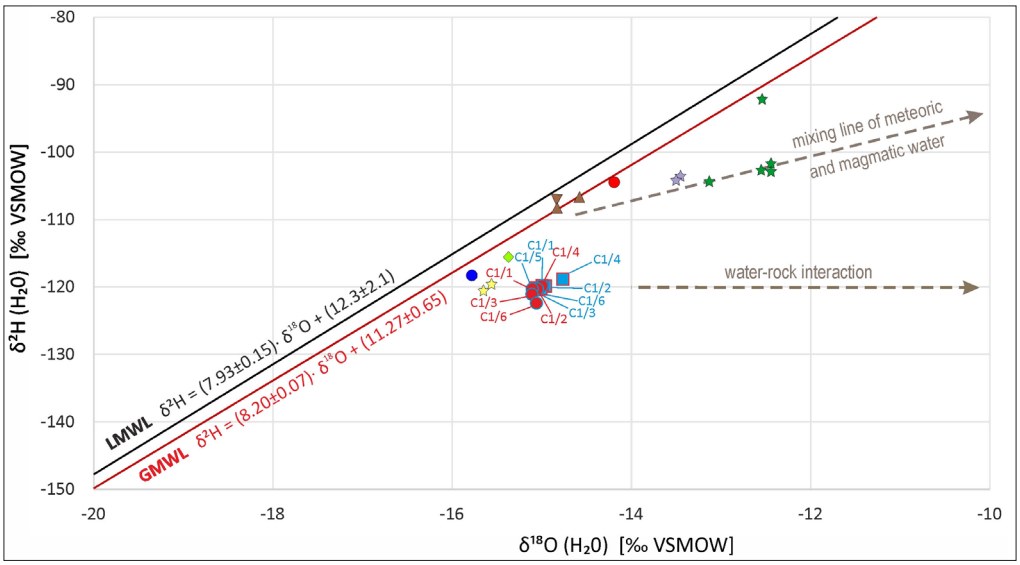

Fig. 11. $\delta^{18}O$ vs. $\delta^{2}H$ plot for waters of the Gruta con Lago and of springs; LMWL after Boschetti et al. (2019) and Valdivielso et al. (2021); GMWL according to Craig (1961), modified by Rozanski et al. (1993); Symbols' meaning as in Figure 4.

The oxygen and hydrogen isotopic composition of waters in Gruta con Lago confirms water-rock interaction along the pathway of underground flow. The presence of trace elements, such as Li, B, Sr and Ba, in the waters of the cave and springs (Supplementary Table S1 and Figure S3) also indicates such interaction. Lithium and boron are present in thermal waters in the Colca River basin

geothermal system, but their content is much higher than in the studied waters (Tyc et al., 2022). Both are related to geothermal fluids and result from rock weathering along their upwelling to the surface. However, in the Mulapampa travertine sector of the geothermal system, some rocks are highly soluble in water (carbonates and evaporites), and bicarbonates, calcium, and sulphates have a large share in the ionic composition. Strontium and barium are substantially essential trace elements.

Selected ratios for the main ions (Ca/SO_4, $Ca/Ca+SO_4$, $HCO_3/Ca+Mg$, $HCO_3+SO_4/Ca+Mg$) in cave and spring waters (presented in Supplementary Table S3) indicate the dominant share of calcite dissolution through water-rock interactions. In 2022, major ion ratios for cave waters were lower, indicating a more significant contribution from gypsum dissolution. At the same time, the waters were not fully equilibrated with the surrounding geochemistry (see $HCO_3+SO_4/Ca+Mg$ for C1/3, C1/5 and C1/6 in Supplementary Table S3), which may be the result of changing redox conditions in the cave itself. Very low Sr/Ca ratio (between 0.004 and 0.006, Supplementary Table S3) indicate rather dominance of dissolved calcite in the whole system.

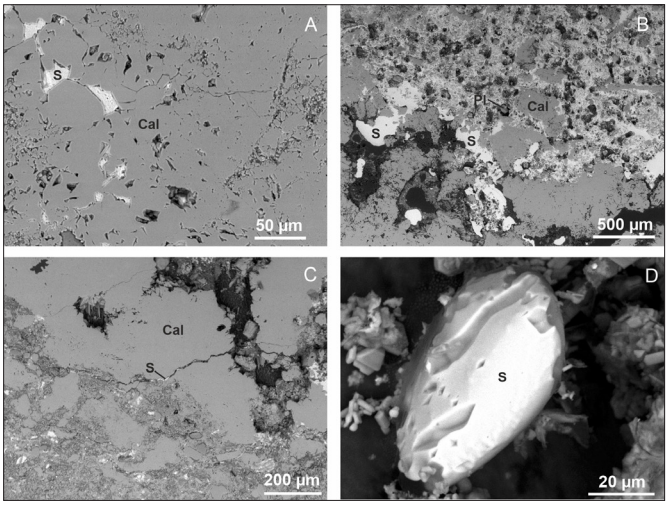

Fig. 12. Native sulfur, gypsum, and detrital plagioclase within travertine samples collected in the peripheries of a small lake at the bottom of the Gruta con Lago (SEM-BSE photographs). A: Native sulfur (S) within calcitic (Cal) travertine; B: Native sulfur and detrital plagioclase (Pl) on the edge of the travertine sample; C: Native sulfur in fractures in travertine (white colour); D: Native sulfur.

Some processes influencing the recorded spatial and temporal variability of water properties (e.g., Eh, pH, Mn content; see Supplementary Table S1 and Figure 5 and Supplementary Fig. S3) are related to redox conditions in the cave. The oxidation state of manganese, the most time- and space-variable trace element in waters of the Gruta con Lago (Supplementary Fig. S3) is mediated by changing redox conditions. In the case of the analyzed cave waters, these conditions are controlled mostly by microbial activity. Microbial mats and biofilms are found in many places in the cave waters (Fig. 5A-C). A special place in this respect is site C1/3 (Fig. 2A), where reducing conditions were found in both periods of the study (Eh with values of -130 and -28 mV; Supplementary Table S1). Additionally, in 2022, bubbling and a rotten egg smell were recorded, indicating degassing of H_2S. In this case, sulfates, i.e. speleogenetic gypsum, are reduced to hydrogen sulfide mediated by bacteria. In travertine samples from the cave's lake (C1/1 in Fig. 2A) and other small water reservoirs in Gruta con Lago native sulfur was detected (Fig. 12). Microscopic examination of their crystals reveals traces of substantial corrosion attributable to the activity of sulfur bacteria (Fig. 12D). The presence of native sulfur in the incompletely dissolved travertine structure may indicate incomplete oxidation of H_2S at low pH, on the other hand buffering of the sulfuric acid by the dissolution of travertine keeps the water pH moderate, in the range of 6-7 (Palmer & Hill, 2019). The effects of changes in redox conditions in the cave, including microbial involvement, recorded in Gruta con Lago are not manifestations of contemporary SAS processes in Mulapampa travertine but only secondary processes after the cessation of possible SAS event in this massif.

Conceptual model of speleogenesis in the Mulapampa travertine

Although we do not yet have dating results to determine the timing of the speleogenesis stages in the Mulapampa travertine, we propose a conceptual model. This model considers possible stages of speleogenesis associated with sulfuric acid (SAS) in the area, including the formation of a travertine cover as a result of subsurface SAS activity within the underlying carbonates. Multiple hypogenic scenarios are considered, all of which emphasize the importance of the geological and geodynamic settings of the Ampato-Sabancaya Volcanic Complex (ASVC) and its related geothermal system. The presence of extensive carbonate formations (Arcurquina Formation) over the magma chamber, combined with active fault zones, is especially critical.

Mantle degassing, as part of magmatic processes, is a significant source of hydrogen sulfide (H_2S). H_2S from this source is abundant in volcanic regions or where deep active magma bodies exist (De Waele & Gutiérrez, 2022; De Waele et al., 2024). One of the best-known examples of SAS caves associated with volcanogenic H_2S is the Sistema Zacatón in Mexico (Gary & Sharp, 2006, 2009; Gary, 2017). The nearby Villa Aldama volcanic complex, located 3 km from the Zacatón Cave area, accelerates carbonate dissolution by increasing the levels of dissolved H_2S and CO_2 in groundwater. This has led to the formation of large phreatic caves of depths reaching 400 m (Gary & Sharp, 2006).

In magmatic volatiles, sulfur exists primarily in the forms of sulfur dioxide (SO_2) and hydrogen sulfide (H_2S), with higher pressure typically favoring H_2S. The disproportionation of SO_2 and the oxidation of H_2S are crucial processes in the production of acids within the hydrothermal systems overlying magma chambers (Li et al., 2024). As a result, geothermal regions with volcanic activity are predisposed to the development of SAS caves in areas where carbonate rocks are adjacent to these systems.

The development of a travertine cover over thick carbonate formations is the first and essential stage

in this process. As mentioned in the introduction, the extensive Mulapampa travertines are thermogenic, forming due to the upwelling of CO_2 and/or H_2S, which then interacted with the thick limestone of the Arcurquina Formation. In both CO_2- and/or H_2S-rich solutions, large phreatic caves formed within the carbonates of the Arcurquina Formation. At this stage, extensive hypogenic processes resulted in the formation of massive travertine at the surface and large subsurface karst systems.

It is difficult to identify direct signatures of the solutions that formed the travertine, making it challenging to distinguish whether they provide evidence of subsurface carbonic or sulfuric acid activity. Examples from Hot Springs, USA, and Sistema Zacatón, Mexico (Hose, 2013), suggest that both scenarios could apply. Even if active SAS occurred within the Arcurquina Formation limestones, the sulfate mineral by-products (e.g., gypsum accumulations) found in Gruta con Lago are not related to this stage of speleogenesis.

In the subsequent stage of speleogenesis, two independent scenarios must be considered: (1) an independent cave system developed in the travertine or (2) the cave system in the Arcurquina Formation continued to enlarge, leading to the collapse and the propagation of sinkholes on the travertine surface. In the first case, cave development could be linked to active sulfuric or carbonic acid enlargement, followed by collapse and the creation of sinkholes at the surface, as observed in present-day caves. It is important to emphasize that, in this scenario, the caves within the travertines were likely formed by hypogenic processes in a CO_2-dominated system. The introduction of H_2S occurred at a later stage and did not contribute directly to the speleogenesis. The massive gypsum accumulations and replacement crusts identified in Gruta con Lago are likely associated with this phase in both scenarios.

An essential factor controlling speleogenesis, particularly the water table position, in both the Arcurquina Formation and Mulapampa travertine, is the incision rate of the Colca River. This process was interrupted several times by extensive lava flows during the Pleistocene due to volcanic activity from the Hualca-Hualca and Ampato volcanoes, which dammed the Colca River valley. Following these volcanic events, the water table was affected, altering the conditions of cave formation. Alongside river incision, the rate of tectonic uplift also plays a role in controlling the water table position in the adjacent massif.

Volcanic activity near the Mulapampa travertine is primarily associated with the Sabancaya volcano, the second most active and youngest volcano in Peru (Machacca et al., 2023). Together with the older Hualca Hualca and Ampato volcanoes, Sabancaya forms the Ampato-Sabancaya Volcanic Complex (ASVC), located east of the study area (Fig. 1A and C; Boixart et al., 2020). The ASVC's eruptive history includes several stages, from the Pleistocene to the present, starting with Hualca Hualca volcano, followed by Ampato, and more recently, Sabancaya (Samaniego et al., 2016).

Benavente et al. (2017) mapped and documented the NW-striking Mucurca-Ampato-Casablanca Fault (MACF), an active reverse fault in the northern part of the study area. Intense volcanic activity persisted for an extended period during the Pleistocene. Based on Samaniego et al. (2016), around 500,000 years ago, Hualca Hualca became inactive, and the Ampato magma chamber, closer to the Mulapampa travertine massif, became active. The MACF likely facilitated the migration of CO_2 and/or H_2S toward the surface, leading to the deposition of massive travertine. This stage likely marked a period of increasing H_2S and CO_2 concentrations in ascending gases and groundwater, playing a critical role in speleogenesis.

CONCLUSIONS

The mineralogical study of Gruta con Lago reveals gypsum as the predominant by-product of sulfuric acid speleogenesis (SAS). Gypsum occurs in various forms, including wall crusts, subaqueous deposits, and thick floor sediments, indicating different stages of cave evolution under both subaerial and subaqueous conditions. Additionally, the presence of celestine suggests secondary mineral formation after the cessation of SAS activity, likely through evaporitic processes.

The preservation of speleogenetic gypsum in Gruta con Lago is attributed to a combination of specific microclimatic conditions within the cave and the region's semi-arid environment. The cave's isolation from modern geomorphological processes, such as annual mudflows that impact other caves in the Mulapampa travertine, has further contributed to the protection of these mineral deposits. This highlights the importance of local environmental stability in preserving SAS mineralogical signatures.

The sulfur and oxygen isotopic composition of gypsum deposits in the Gruta con Lago Cave strongly indicates a speleogenetic process driven by the oxidation of sulfide (H_2S). The light $\delta^{34}S$ values found in the cave gypsum support the hypothesis that subaqueous and subaerial oxidation of H_2S, followed by reactions with H_2SO_4 and travertine, played a key role in the formation of sulfate deposits. This isotopic evidence provides a clear signature of former sulfuric acid activity within the cave system.

The geochemistry of waters in the Gruta con Lago and Huambo springs is influenced by the geothermal system in the Colca River basin, but differs distinctly from the thermal springs in that area. The waters in Gruta con Lago show signs of water-rock interaction along their underground flow, with isotopic compositions indicating interactions with the surrounding geology. The presence of trace elements such as lithium, boron, strontium, and barium supports this, though their concentrations are lower than in the geothermal system. Dissolution of calcite and gypsum dominates the cave water's chemical composition, with calcite being the primary dissolved mineral.

Observed spatial and temporal variability of water properties in the Gruta con Lago Cave is driven by redox conditions, primarily influenced by microbial

activity. Processes such as the reduction of sulfates to hydrogen sulfide and the partial oxidation of H_2S are mediated by sulfur bacteria, leading to the formation of native sulfur and the corrosion of travertine structures. However, these changes in redox conditions are secondary processes, occurring after the cessation of a potential SAS event in the cave's travertine formations.

The development of the Mulapampa travertine and associated speleogenesis is highly influenced by the unique geological and volcanic conditions of the Ampato-Sabancaya Volcanic Complex (ASVC). Hypogenic processes driven by magmatic CO_2 and H_2S upwelling through the underlying carbonates of the Arcurquina Formation have played a crucial role in forming both the surface travertine deposits and the subsurface karst systems. The presence of active volcanic systems, fault zones, and geothermal activity significantly enhances the dissolution of carbonates and the subsequent formation of large phreatic caves.

The speleogenesis of the Mulapampa travertine follows a complex, multi-stage process influenced by both sulfuric and carbonic acid-driven mechanisms. While it is challenging to distinguish between the contributions of sulfuric and carbonic acids in the formation of the travertine, evidence from similar geothermal regions (such as Sistema Zacatón in Mexico) suggests that both processes likely contributed to the development of the cave systems. Future research, particularly dating of the speleogenetic stages and further analysis of sulfate mineral by-products, will be crucial in refining the conceptual model of this unique hypogenic system.

ACKNOWLEDGMENTS

The article is our tribute to the memory of Alexander B. Klimchouk, who made so much to develop the concept of hypogene karst. This research was funded by National Science Centre (Poland), grant No 2020/39/B/ST10/00042, and Institute of Earth Sciences, University of Silesia, Poland. For the purpose of Open Access, the authors have applied a CC-BY public copyright license to any Author Accepted Manuscript (AAM) version arising from this submission. Constructive and valuable comments from the Editors, Jo De Waele and Bogdan P. Onac, and three reviewers have significantly improved the manuscript. We want to thank Andrzej Paulo, and Jerzy Żaba for help in the field, Beata Gebus-Czupyt for conducting isotope analysis, Pablo Masías, Melvin Benavente, Paul Navarro, Eduardo Benavente Escarza, and Abdul Huamaní Escarza for logistic assistance and their help in contacts with local communities. We are grateful to the local community of Huambo for kindly giving us access to work and for help in the field.

Authorship statement: AT: conceptualization, original draft preparation, methodology, field work, data curation, formal analysis, writing, review and editing, figures. KG: conceptualization, methodology, field work, data curation, formal analysis, writing, review, figures, funding acquisition. JC: methodology, field work, formal analysis, review, laboratory work, figures. KW: methodology, data curation, laboratory work, review, figures.

REFERENCES

Benavente, C., Delgado, G., García, B., Aguirre, E., Audin, L., 2017. Neotectónica, evolución del relieve y peligro sísmico en la Región Arequipa. INGEMMET. Boletín, Serie C, 64. Geodinamica e Ingeniería Geológica, 370 p. https://hdl.handle.net/20.500.12544/1223

Boschetti, T., Cifuentes, J., Iacumin, P., Selmo, E.M., 2019. Local Meteoric Water Line of Northern Chile (18° S–30° S): an application of error-in-variables regression to the oxygen and hydrogen stable isotope ratio of precipitation. Water, 11(4), 791. https://doi.org/10.3390/w11040791

Boixart, G., Cruz, L.F., Miranda Cruz, R., Euillades, P.A., Euillades, L.D., Battaglia, M., 2020. Source model for Sabancaya volcano constrained by DInSAR and GNSS surface deformation observation. Remote Sensing, 12(11), 1852. https://doi.org/10.3390/rs12111852

Buck, M.J., Ford, D.C., Schwarcz, H.P., 1994. Classification of cave gypsum deposits derived from oxidation of H_2S. In: Sasowsky, I.D., Palmer, M.V. (Eds.), Breakthroughs in karst geomicrobiology, Colorado Springs. Karst Water Institute, Special Publication 1, 5-9.

Caldas, J., 1993. Geología de los cuadrángulos de Huambo y Orcopampa, Hojas: 32-r, 31-r-[Boletín A 46]. https://repositorio.ingemmet.gob.pe/handle/20.500.12544/166

Chervyatsova, O.Y., Potapov, S.S., Kuzmina, L.Y., Dublyansky, Y.V., Sadykov, S.A., Kiseleva, D.V., Okuneva, T.G., Dzhabrailov, S.-E.M., Samokhin, G.V., 2020. Sulfuric acid speleogenesis in the North Caucasus: Sharo-Argun valley Caves (Chechen Republic, Russia). Geomorphology, 369, 107346. https://doi.org/10.1016/j.geomorph.2020.107346

Ciesielczuk, J., Żaba, J., Bzowska, G., Gaidzik, K., Głogowska, M., 2013. Surface mineralization at the geyser near Pinchollo, southern Peru. Journal of South American Earth Sciences, 53, 186-193. https://doi.org/10.1016/j.jsames.2012.06.016

Craig, H., 1961. Isotopic variations in meteoric waters. Science, 133, 1702-1703. https:// doi.org/10.1126/science.133.3465.1702

Damm, B., 1968. Ein Riesenkegel aus Travertin (NW Iran). Der Aufschluss, 11, 323-332.

D'Angeli, I., Carbone, C., Nagostinis, M., Parise, M., Vattano, M., Madonia, G., De Waele, J. (2018). New insights on secondary minerals from Italian sulfuric acid caves. International Journal of Speleology, 47(3), 271-291. https://doi.org/10.5038/1827-806X.47.3.2175

D'Angeli, I.M., Nagostinis, M., Carbone, C., Bernasconi, S.M., Polyak, V.J., Peters, L., McIntosh,W.C., De Waele, J., 2019a. Sulfuric acid speleogenesis in the Majella Massif (Abruzzo, Central Apennines, Italy). Geomorphology, 333, 167-179. https://doi.org/ 10.1016/j.geomorph.2019.02.036

D'Angeli, I. M., Parise, M., Vattano, M., Madonia, G., Galdenzi, S., De Waele, J., 2019b. Sulfuric acid caves of Italy: A review. Geomorphology, 333, 105-122. https://doi.org/ 10.1016/j.geomorph.2019.02.025

Delgado, F., Zerathe, S., Schwartz, S., Mathieux, B., Benavente, C., 2022. Inventory of large landslides along the Central Western Andes (ca. 15–20 S): landslide

distribution patterns and insights on controlling factors. Journal of South American Earth Sciences, 116, 103824. https://doi.org/10.1016/j.jsames.2022.103824

De Waele, J., Audra, P., Madonia, G., Vattano, M., Plan, L., D'Angeli, I.M., Bigot, J.-Y., Nobécourt, J.-C., 2016. Sulfuric acid speleogenesis (SAS) close to the water table: examples from southern France, Austria, and Sicily. Geomorphology, 253, 452-467. https://doi.org/10.1016/j.geomorph.2015.10.019

De Waele, J., Gutiérrez, F., 2022. Karst hydrogeology, geomorphology and caves. Wiley, Chichester, 912 p. https://doi.org/10.1002/9781119605379

De Waele, J., D'Angeli, I.M., Audra, P., Plan, L., Palmer, A.N., 2024. Sulfuric acid caves of the world: A review. Earth-Science Reviews, 250, 104693. https://doi.org/10.1016/ j.earscirev.2024.104693

Egemeier, S.J., 1981. Cavern development by thermal waters. National Speleological Society Bulletin, 43, 31-51.

Forti, P., Benedetto, C., Costa, G., 1993. Las Brujas cave (Malargue, Argentina): an example of the oil pools control on the speleogenesis. Theoretical and Applied Karstology, 6, 87-93.

Gaidzik, K., Żaba, J., Ciesielczuk, J., 2020. Tectonic control on slow-moving Andean landslides in the Colca Valley, Peru. Journal of Mountain Science, 17(8), 1807-1825. https://doi.org/10.1007/s11629-020-6099-y

Gaidzik, K., Więsek, M., 2021. Seismo-lineaments and potentially seismogenic faults in the overriding plate of the Nazca-South American subduction zone (S Peru). Journal of South American Earth Sciences, 109, 103303. https://doi:10910.1016/j.jsames.2021.103303

Galdenzi, S., Maruoka, T., 2003. Gypsum deposits in the Frasassi Caves, central Italy. Journal of Cave and Karst Studies, 65, 111-125.

Galdenzi, S., Maruoka, T., 2019. Sulfuric acid caves in Calabria (South Italy): Cave morphology and sulfate deposits. Geomorphology, 328, 211-221. https://doi.org/10.1016/j.geomorph.2018.12.014

Gałaś, A., 2014. Petrology and new data on the geochemistry of the Andahua volcanic group (Central Andes, southern Peru). Journal of South American Earth Sciences, 56, 301-315. https://doi.org/10.1016/j.jsames.2014.09.012

Gary, M.O., 2017. Sistema Zacatón: volcanically controlled hypogenic karst, Tamaulipas, Mexico. In: Klimchouk, A.B., Audra, P., Palmer, A.N., De Waele, J., Auler, A. (Eds.), Hypogene karst regions and caves of the world. Springer, Cham, p. 769-782. https://doi.org/10.1007/978-3-319-53348-3_52

Gary, M.O., Sharp, J.M., 2006. Volcanogenic karstification of Sistema Zacatón, Mexico. Geological Society of America, Special Paper, 404, 79-89. https://doi.org/10.1130/2006.2404(08)

Gary, M.O., Sharp, J.M., 2009. Volcanogenic karstification: implications of this hypogene process. In: Stafford, K.W., Land, L., Veni, G. (Eds.), Advances in hypogene karst studies. National Cave and Karst Research Institute Symposium 1, Carlsbad, NM, p. 27-39.

Gradziński, M., Bella, P., Holúbek, P., 2018. Constructional caves in freshwater limestone: A review of their origin, classification, significance and global occurrence. Earth-Science Reviews, 185, 179-201. https://doi.org/10.1016/j.earscirev.2018.05.018

Hill, C.A., 1987. Geology of Carlsbad Cavern and other caves in the Guadalupe Mountains, New Mexico and Texas. New Mexico Bureau of Mines & Mineral Resources Bulletin 117, 1-150. https://doi.org/10.58799/B-117

Hill, C.A., 1995. Sulfur redox reactions: hydrocarbons, native sulfur, Mississippi Valley type deposits, and sulfuric acid karst in the Delaware Basin, New Mexico and Texas. Environmental Geology, 25, 16-23. https://doi.org/10.1007/BF01061826

Hill, C.A., 2000. Sulfuric acid hypogene karst in the Guadalupe Mountains of New Mexico and West Texas, USA. In: Klimchouk, A.B., Ford, D.C., Palmer, A.N., Dreybrodt, W. (Eds.), Speleogenesis: Evolution of karst aquifers. Huntsville, AL, National Speleological Society, p. 309-316.

Hose, L.D., 2013. Karst geomorphology: Sulfur karst processes. In: Frumkin, A., Shroder, J. (Eds.), Treatise on geomorphology. Academic Press, p. 29-37. https://doi.org/10.1016/B978-0-12-374739-6.00117-2

Hose, L.D., Palmer, A.N., Palmer, M.V., Northup, D.E., Boston, P.J., Du Chene, H.R., 2000. Microbiology and geochemistry in a hydrogen-sulphide-rich karst environment. Chemical Geology, 169(3-4), 399-423. https://doi.org/10.1016/S0009-2541(00)00217-5

Klimchouk, A.B., 2019. Speleogenesis – Hypogene. In: White, W.B., Culver, D.C., Pipan, T. (Eds.), Encyclopedia of caves (3rd Ed.). Elsevier/Academic Press, Amsterdam, p. 974-978. https://doi.org/10.1016/B978-0-12-814124-3.00114-X

Klimchouk, A.B., Evans, D., Milanovic, S., Bittencourt, C., Sanchez, M., Aguirre, F.C., 2023. Hypogene speleogenesis related to porphyry magmatic intrusions and its influence on subsequent karst evolution in the Peruvian high Andes. Geomorphology, 420, 108488. https://doi.org/10.1016/j.geomorph.2022.108488

Laurent, D., Barré, G., Durlet, C., Cartigny, P., Carpentier, C., Paris, G., Collon, P., Pironon, J., Gaucher, E.C., 2023. Unravelling biotic versus abiotic processes in the development of large sulfuric-acid karsts. Geology, 51(3), 262-267. https://doi.org/10.1130/G50658.1

Li, B., Kong, Q., Liao, F., Wang, G., Liu, F., Guo, L., Liu, C., Shi, Z., 2024. Sulphur evolution in acidic and alkaline geothermal water related to magma in the Rehai geothermal field in the southeastern Tibet Plateau based on stable hydrogen, oxygen, sulphur isotopes. Geothermics, 119, 102931. https://doi.org/10.1016/j.geothermics.2024.102931

Machacca, R., Lesage, P., Tavera, H., Pesicek, J.D., Caudron, C., Torres, J.L., Puma, N., Vargas, K., Lazarte, I., Rivera, M., Burgisser, A., 2023. The 2013–2020 seismic activity at Sabancaya Volcano (Peru): long lasting unrest and eruption. Journal of Volcanology and Geothermal Research, 435, 107767. https://doi.org/10.1016/j.jvolgeores.2023.107767

Mansor, M., Harouaka, K., Gonzales, M.S., Macalady, J.L., Fantle, M.S., 2018. Transport induced spatial patterns of sulfur isotopes ($\delta^{34}S$) as biosignatures. Astrobiology, 18, 59-72. https://doi.org/10.1089/ast.2017.1650

Mayer, B., 2005. Assessing sources and transformations of sulphate and nitrate in the hydrosphere using isotope techniques. In: Aggarwal, P.K., Gat, J.R., Froehlich, K.F.O. (Eds.), Isotopes in the water cycle: Past, present and future of a developing science. Springer, p. 67-89. https://doi.org/10.1007/1-4020-3023-1_6

National Service of Meteorology and Hydrology of Peru, https://www.senamhi.gob.pe/?&p=estaciones [accessed: April 15, 2024]

Onac, B.P., Hess, J.W., White, W.B., 2007. The relationship between the mineral composition of speleothems and mineralization of breccia pipes: evidence from Corkscrew Cave, Arizona, USA. Canadian Mineralogy, 45(5), 1177–1188. https://doi.org/10.2113/gscanmin.45.5.1177

Onac, B.P., Sumrall, J.G., Tamas, T., Povara, I., Kearns, J., Darmiceanu, V., Veres, D.S., Lascu, C., 2009. The relationship between cave minerals and H_2S-rich thermal waters along the Cerna Valley (SW Romania). Acta Carsologica, 38(1), 67-79. https://doi.org/10.3986/ac.v38i1.135

Onac, B.P., Wynn, J.G., Sumrall, J.B., 2011. Tracing the sources of cave sulfates: a unique case from Cerna Valley, Romania. Chemical Geology, 288(3-4), 105-114. https://doi.org/10.1016/j.chemgeo.2011.07.006

Palmer, A.N., 2013. Sulfuric acid caves. In: Frumkin, A., Shroder, J. (Eds.), Treatise on geomorphology. Elsevier, p. 241-257. https://doi.org/10.1016/B978-0-12-374739-6.00133-0

Palmer, A.N., Hill, C.A., 2019. Sulfuric acid caves. In: White, W.B., Culver, D.C., Pipan, T. (Eds.), Encyclopedia of caves (3rd Ed.). Elsevier/Academic Press, Amsterdam, p. 1053-1062. https://doi.org/10.1016/B978-0-12-814124-3.00122-9

Palmer, A.N., Palmer, M.V., 2004. Sulfate-carbonate interactions in the development of karst. Northeastern Geology and Environmental Sciences, 26(1-2), 93-106.

Palmer, M.V., Palmer, A.N., 2012. Petrographic and isotopic evidence for late-stage processes in sulfuric acid caves of the Guadalupe Mountains, New Mexico, USA. International Journal of Speleology, 41(2), 231-250. https://doi.org/10.5038/1827-806X.41.2.10

Paulo, A., Ciesielczuk, J., Gaidzik, K., Żaba, J. Gaweł, A., Bzowska, G., 2013. Thermal alterations of the Ashua formation at the contact with a porphyry intrusion (Huambo, south Peru): a reconnaissance study. Boletín de la Sociedad Geológica del Perú, 107, 27-30.

Paulo, A., Ciesielczuk, J., Racki, G., Żaba, J., Gaidzik, K., 2019. Depositional environment and probable source of detritus in the Upper Cretaceous red-bed Ashua Formation (Peru). Przegląd Geologiczny, 67, 189-191 [in Polish, English summary]. https://doi.org/10.7306/2019.17

Pentecost, A., 2005. Travertine. Springer, Berlin, 460 p.

Pentecost, A., Viles, H.A., 1994. A review and reassessment of travertine classification. Geographie Physique et Quaternaire, 48, 305-314. https://doi.org/10.7202/033011ar

Piccini, L., DeWaele, J., Galli, E., Polyak, V.J., Bernasconi, S.M., Asmerom, Y., 2015. Sulphuric acid speleogenesis and landscape evolution: Montacchio Cave, Albegna River Valley (southern Tuscany, Italy). Geomorphology, 229, 134-143. https://doi.org/10.1016/j.geomorph.2014.10.006

Pisarowicz, J.A., 1994. Cueva de Villa Luz − an active case of H_2S speleogenesis. In: Sasowsky, I.D., Palmer, M.V. (Eds.), Breakthroughs in karst geomicrobiology. Colorado Springs, p. 60-62.

Polyak, V.J., Provencio, P., 2001. By-product materials related to H_2S-H_2SO_4-influenced speleogenesis of Carlsbad, Lechuguilla, and other caves of the Guadalupe Mountains, New Mexico. Journal of Cave and Karst Studies, 63(1), 23-32.

Polyak, V.J., Forbes, J.R., Spilde, M.N., Provencio, P., Cochran, J.R., Asmerom, Y., 2024. CO_2 hypogene speleogenesis in an endogenic travertine system, Mesa del Oro, New Mexico, USA. International Journal of Speleology, 53(2), 159-167. https://doi.org/10.5038/1827-806X.53.2.2502

Romero Fernández, D., Ticona Turpo, P., 2003. Memoria descriptiva de la revisión y actualización del cuadrángulo de Huambo (32-r). Escala 1: 50.000. https://repositorio.ingemmet.gob.pe/handle/20.500.12544/2056

Rozanski, K., Araguás-Araguáo, L., Gonfiantini, R., 1993. Isotopic patterns in modern global precipitation. In: Climate change in continental isotopic records, Geophysical Monograph, 78, 36 p.

Samaniego, P., Rivera, M., Mariño, J., Guillou, H., Liorzou, C., Zerathe, S., Delgado, R., Valderrama, P., Scao, V., 2016. The eruptive chronology of the Ampato–Sabancaya volcanic complex (Southern Peru). Journal of Volcanology and Geothermal Research, 323, 110-128. https://doi.org/10.1016/j.jvolgeores.2016.04.038

Sancho, C., Osácar, C., Peña, J.L., Mandado, J., Mikkan, R., Quinif, Y., 2002. Gypsum cave deposits in the Caverna de Las Brujas (Andean Range, Mendoza Province, Argentina): Origin and palaeoenvironmental significance. Boletín Geológico y Minero, 113(4), 339-349.

Sancho, C., Peña, J.L., Mikkan, R., Osácar, C., Quinif, Y., 2004. Morphological and speleothemic development in Brujas Cave (Southern Andean range, Argentine): palaeoenvironmental significance. Geomorphology, 57(3), 367–384. https://doi.org/10.1016/S0169-555X(03)00166-1

Sørensen, E. V., Holm, P.M., 2008. Petrological inferences on the evolution of magmas erupted in the Andagua Valley, Peru (Central Volcanic Zone). Journal of volcanology and geothermal research, 177(2), 378-396. https://doi.org/10.1016/j.jvolgeores.2008.05.021

Temovski, M., Futó, I., Túri, M., Palcsu, L., 2018. Sulfur and oxygen isotopes in the gypsum deposits of the Provalata sulfuric acid cave (Macedonia). Geomorphology, 315, 80-90. https://doi.org/10.1016/j.geomorph.2018.05.010

Tyc, A., Gaidzik, K., Ciesielczuk, J., Masías, P., Paulo, A., Postawa, A., Żaba, J., 2022. Thermal springs and active fault network of the central Colca River basin, Western Cordillera, Peru. Journal of Volcanology and Geothermal Research, 424, 107513. https://doi.org/10.1016/j.jvolgeores.2022.107513

USGS Earth Explorer Portal. https://earthexplorer.usgs.gov [accessed: June 15, 2022]

UNESCO. Takht-e Soleyman. https://whc.unesco.org/uploads/nominations/1077.pdf [accessed: February 12, 2024.

Valdivielso, S., Vázquez-Suñé, E., Custodio, E., 2021. Isotopía ambiental de las precipitaciones y de las aguas superficiales y subterráneas en los Andes Centrales: Revisión. Boletín Geológico y Minero, 132(1-2), 147-156. https://doi.org/10.21701/bolgeomin.132.1-2.015

Woszczycka, M., Gaidzik K., Anccasi Figueroa R. M., Mendecki M., Benavente C., 2024. Unraveling the complex interplay: exploring the relationships between seismic and volcanic activities in the Colca River area using the Coulomb Stress Transfer. Seismological Research Letters, 95(4), 2464-2484. https://doi.org/10.1785/0220230261

Zavala, B., Vilchez, M., Rosado, M., Pari, W., Peña, F., 2014. Estudio geoambiental en la Cuenca del Rio Colca. INGEMMET Bol. Serie C, 57, p. 1-222.

Zerkle, A.L., Jones, D.S., Farquhar, J., Macalady, J.L., 2016. Sulfur isotope values in the sulfidic Frasassi cave system, Central Italy: a case study of a chemolithotrophic S-based ecosystem. Geochimica et Cosmochimica Acta, 173, 373–386. https://doi.org/10.1016/j.gca.2015.10.028